RMetS
Royal Meteorological Society

Similarity theory based on the Dougherty–Ozmidov length scale

Andrey A. Grachev,[a,b]* Edgar L Andreas,[c] Christopher W. Fairall,[a] Peter S. Guest[d] and P. Ola G. Persson[a,b]

[a]*NOAA Earth System Research Laboratory, Boulder, CO, USA*
[b]*Cooperative Institute for Research in Environmental Sciences, University of Colorado, Boulder, CO, USA*
[c]*NorthWest Research Associates, Inc., Lebanon, NH, USA*
[d]*Naval Postgraduate School, Monterey, CA, USA*

*Correspondence to: A. A. Grachev, NOAA Earth System Research Laboratory, 325 Broadway, R/PSD3, Boulder, CO 80305-3337, USA. E-mail: Andrey.Grachev@noaa.gov

This article describes a local similarity theory for developed turbulence in the stably stratified boundary layer that is based on the Brunt–Väisälä frequency and the dissipation rate of turbulent kinetic energy instead of the turbulent fluxes used in the traditional Monin–Obukhov similarity theory. Based on dimensional analysis (Pi theorem), it is shown that any properly scaled statistics of the small-scale turbulence are universal functions of a stability parameter defined as the ratio of a reference height z and the Dougherty–Ozmidov length scale, which in the limit of z-less stratification is linearly proportional to the Obukhov length scale. Measurements of atmospheric turbulence made at five levels on a 20 m tower over the Arctic pack ice during the Surface Heat Budget of the Arctic Ocean experiment (SHEBA) are used to examine the behaviour of different similarity functions in the stable boundary layer. In the framework of this approach the non-dimensional turbulent viscosity is equal to the gradient Richardson number, whereas the non-dimensional turbulent thermal diffusivity is equal to the flux Richardson number. These results are a consequence of the approximate local balance between production of turbulence by shear in the mean flow and viscous dissipation. The turbulence framework based on the Brunt–Väisälä frequency and the dissipation rate of turbulent kinetic energy may have practical advantages for estimating turbulence when the fluxes are not directly available.

Key Words: Dougherty–Ozmidov length scale; mixing efficiency; Monin–Obukhov similarity theory; oceanic vertical mixing; stable boundary layer; z-less similarity

Received 4 April 2014; Revised 8 October 2014; Accepted 22 October 2014; Published online in Wiley Online Library

1. Introduction

Sixty years ago, Monin and Obukhov (1954) suggested a similarity theory that is the commonly accepted approach to describe turbulence in the near-surface atmosphere. The basis of the Monin–Obukhov similarity theory (MOST) had been laid earlier by Obukhov's (1946) fundamental article (e.g. see historical survey by Foken, 2006). Among other things Obukhov (1946) proposed a buoyancy length scale L ('Obukhov length') which plays a central role in the MOST.

Based on dimensional analysis (Pi theorem), the MOST states that turbulent fluxes of momentum and heat (in the general case buoyancy) are the primary governing (independent) variables that, along with the buoyancy parameter β, define how other (dependent) variables (e.g. vertical gradients, variances, etc.) in the atmospheric surface layer depend on the height z. Originally the MOST was based on the assumption that the turbulent fluxes are constant with height and equal to the surface values in the layer conventionally called a surface or constant-flux layer, that is, 'surface scaling'. Subsequently, Nieuwstadt (1984) demonstrated that in the stable boundary layer (SBL) the assumption of height-independent fluxes is not necessary and Monin–Obukhov similarity can be redefined in terms of the local fluxes at height z (i.e. z-dependent fluxes) rather than on the surface values, which is known as 'local scaling'. In fact, Nieuwstadt deprived the turbulent fluxes of their 'privileged role' and paved the way to construct a local similarity theory in the SBL based on governing variables other than the fluxes.

The Pi theorem used in the MOST provides only a general methodology, and the choice of the primary governing variables is not unique. Presumably, Smeets *et al.* (2000) first discussed a similarity theory based on non-MOST governing parameters. In their article, Smeets *et al.* modified the MOST by replacing the friction velocity with the standard deviation of the vertical wind-speed component σ_w to study the SBL over a glacier surface in a predominantly katabatic flow.

Sorbjan (2006) proposed alternative local scaling for the SBL based on σ_w, the Brunt–Väisälä frequency N, and β (a

buoyancy length-scale defined as σ_w/N) and introduced the concept of gradient-based scaling. Subsequently, Sorbjan (2008, 2010) suggested three more gradient-based scaling systems. The gradient-based similarity approach removes turbulent fluxes as governing parameters and replaces them with vertical gradients of mean wind speed and potential temperature. As a result, the gradient Richardson number, *Ri*, appears as a stability parameter instead of the Monin–Obukhov stability parameter z/L. Sorbjan (2006, 2008, 2010) and Sorbjan and Grachev (2010) discussed different universal functions plotted versus *Ri* based on field data. Obukhov length L, the gradient Richardson number *Ri*, the Brunt–Väisälä frequency N, and other variables mentioned here will be defined in sections 3 and 4.

In this article, we further develop Sorbjan's (2006) ideas and suggest a similarity theory for the stably stratified boundary layer based on N and the dissipation rate of turbulent kinetic energy ε (cf. Sorbjan and Balsley, 2008). A buoyancy length scale constructed from N and ε was originally suggested by Dougherty (1961) and Ozmidov (1965) and herein is referred to as the Dougherty–Ozmidov length scale. It is also known as the Ozmidov length and is widely used in oceanography to describe small-scale turbulence. In contrast to the gradient-based scaling, we consider various similarity functions versus both the Richardson number and a stability parameter defined as the ratio of a reference height z and the Dougherty–Ozmidov length scale, which plays the role of the Obukhov length in the proposed approach. We use the extensive measurements of atmospheric turbulence from the Surface Heat Budget of the Arctic Ocean experiment (SHEBA) described in section 2 to examine the Dougherty–Ozmidov length scale and to derive similarity functions.

2. Data and data processing

Turbulence measurements made over the Arctic pack ice during the SHEBA took place in the Beaufort Gyre from 2 October 1997 to 11 October 1998. Andreas *et al.* (2006, 2010a, 2010b, 2013), Persson *et al.* (2002), Persson (2012) and Grachev *et al.* (2005, 2007a, 2008, 2013) describe the SHEBA site, various measurements over the Arctic sea ice, data processing, accuracy of measurements, instrument calibration, etc. Here we provide some relevant information about the turbulence and profile measurements in the near-surface atmosphere during the SHEBA.

Turbulence statistics (fluxes, variances, spectra, cospectra) and mean meteorological data were continuously measured on a 20 m main tower at five levels, hereafter levels 1–5, nominally $z_1 \approx 2.2$ m, $z_2 \approx 3.2$ m, $z_3 \approx 5.1$ *m*, $z_4 \approx 8.9$ m and $z_5 \approx 18.2$ m (but 14 m during most of the winter). Each level of the tower was instrumented with identical Applied Technologies, Inc. (ATI), three-axis sonic anemometer/thermometers (K-probe) that sampled at 10 Hz and a Väisälä HMP-235 temperature and relative humidity (T/RH) probes. An Ophir fast-response infrared hygrometer was mounted on a 3 m boom at an intermediate level (about 8 m) just below level 4. Although a sonic anemometer/thermometer measures the so-called 'sonic' temperature, which is close to the virtual temperature, the moisture correction in sonic temperature is usually small for Arctic conditions (see estimate in Grachev *et al.*, 2005, p. 205).

The 'slow' T/RH probes provided air temperature and relative humidity measurements at five levels and were used to evaluate the vertical temperature and humidity gradients. The mean wind speed and wind direction were derived from the sonic anemometers in a streamline coordinate system, whereby we performed two rotations on the sonic measurements that forced the mean lateral and vertical wind-speed components to zero (Kaimal and Finnigan, 1994, section 6.6). Vertical gradients of the mean wind speed, potential temperature and specific humidity that appear here were obtained by fitting a second-order polynomial through the 1-h-averaged profiles followed by evaluating the derivative with respect to z for levels 1–5 (Grachev *et al.*, 2005, their eq. (8)).

Hourly averaged turbulent fluxes and variances at each level were derived through the frequency integration of the appropriate cospectra and spectra, which were normally computed from seven overlapping 13.65 min data blocks (corresponding to 2^{13} data points) and then averaged over 1 h (see other details in Persson *et al.*, 2002). One-hour averaging intervals are required to reduce excessive data scatter in the similarity relationships. To separate the contributions from mesoscale motions to the calculated eddy-correlation fluxes, we applied a low-frequency cut-off at 0.0061 Hz (the sixth spectral value or a period of about 3 min) on the cospectra as a lower limit of integration; the upper limit of integration is 5 Hz, the Nyquist frequency. The low-frequency cut-off for turbulent contributions is chosen to lie in the spectral gap between the small- and large-scale contributions to the total transport (see spectra and cospectra plots in Grachev *et al.* (2005, figure 8), Grachev *et al.* (2008, figure 3), and Grachev *et al.* (2013, figures 1–4)).

Several data-quality indicators based on objective and subjective methods have been applied to the original flux data (e.g. Grachev *et al.*, 2007a, p. 319). In particular, to avoid a possible flux loss caused by inadequate frequency response and sensor separations, we omitted data with a local wind speed less than 1 m s^{-1}. In addition, data with a temperature difference between the air (at median level) and the snow surface less than 0.5 °C have also been omitted to avoid the large uncertainty in determining the sensible heat flux in near-isothermal conditions.

However, despite the data-quality control (QC), there are almost always outliers that are noticeably inconsistent with the rest of the dataset, in particular, because they are affected by other phenomena that are not described by similarity theory. To remove spurious or near-zero data points, we further checked the data prior to evaluating similarity functions in order to remove indeterminate forms such as zero divided by zero. Following the QC recommendations by Klipp and Mahrt (2004) and Sanz Rodrigo and Anderson (2013), we set minimum thresholds for the kinematic momentum flux (0.0002 m^{2}s^{-2}), temperature flux (0.0002 K m s^{-1}), standard deviation of each wind-speed component (0.01 m s^{-1}), standard deviation of air temperature (0.01 K), vertical gradients of mean velocity (0.001 s^{-1}) and mean temperature (0.001 K m^{-1}), and dissipation rate of turbulent kinetic energy (0.0003 m^2 s^{-3}). Note that the thresholds for the fluxes and standard deviation are also required in order to avoid amplitude resolution problems (Vickers and Mahrt, 1997, their figure 1(b)). As a result, only about 23% of the original SHEBA dataset for five levels under stable conditions are retained for the analysis.

Resolution of turbulent fluctuations for ATI sonic anemometers as well as for most other sonic anemometers (e.g. Young 81000, Gill WindMaster) is $u', v', w' \sim 0.01$ m s^{-1} for wind speed components and $\theta' \sim 0.01$ K for sonic temperature. Thus, minimum thresholds of the momentum and temperature fluxes can be estimated as $<u'w'> \sim 10^{-4}$ m^2 s^{-2} and $<w'\theta'> \sim 10^{-4}$ K m s^{-1}, respectively. Although our QC thresholds for the fluxes and standard deviation are less rigorous than those used by Klipp and Mahrt (2004) and Sanz Rodrigo and Anderson (2013), we also imposed additional restrictions on the gradient and flux Richardson numbers (see below).

In the current study, the dissipation rate of turbulent kinetic energy ε was estimated based on a common method for measuring ε in a turbulent flow that assumes the existence of an inertial subrange associated with a Richardson–Kolmogorov cascade. Note that the various estimates of ε are valid only for a locally isotropic inertial subrange (see Gargett *et al.*, 1984; Albertson *et al.*, 1997; Biltoft, 2001; Chamecki and Dias, 2004; Piper and Lundquist, 2004; Lien and D'Asaro, 2006 for discussion). The one-dimensional wavenumber energy spectrum of the longitudinal velocity component in the inertial subrange has the form

$$F_u(k) = \alpha \varepsilon^{2/3} k^{-5/3}, \tag{1}$$

where k is the wavenumber and α is the Kolmogorov constant ($\alpha \approx 0.5$–0.6; e.g. Kaimal and Finnigan, 1994); we adopt a value $\alpha = 0.55$ for our study.

Spatial scales and the wavenumber spectrum in Eq. (1) should be converted, respectively, into frequency scales and frequency spectrum, which is traditionally what a sonic anemometer measures. By using Taylor's frozen turbulence hypothesis, $k = 2\pi f/U$ (where f is frequency and U is mean wind speed), the wavenumber spectrum in the inertial subrange (Eq. (1)) can be written in terms of frequency as follows:

$$S_u(f) = \alpha(U/2\pi)^{2/3}\varepsilon^{2/3}f^{-5/3}. \tag{2}$$

Frequency $S_u(f)$ and wavenumber $F_u(k)$ spectra are related to each other through $fS_u(f) = kF_u(k)$ (Kaimal and Finnigan, 1994). If the turbulence is locally isotropic, the spectra of lateral and vertical velocity components are 4/3 of the longitudinal velocity; that is,

$$S_v(f) = S_w(f) = (4/3)S_u(f). \tag{3}$$

Based on Eqs (2) and (3), we derived the dissipation rate of turbulent kinetic energy ε in this study separately from the spectra for each velocity component (u', v', and w') in the frequency domain 0.49–0.74 Hz located within the inertial subrange. We then took the median of these three values as the representative dissipation rate. With this procedure, we avoided the influence of possible spectral spikes on the estimation of the dissipation rate (see figures 1 and 3 in Grachev *et al.*, 2013) and reduced sampling error. As our estimates of ε are based on Eqs (1)–(3), data without the Richardson–Kolmogorov cascade should be filtered out. This study follows Grachev *et al.* (2013) and imposes restrictions on the gradient and flux Richardson numbers, *Ri* and *Rf*, such that we excluded data points if both *Ri* and *Rf* exceed a critical value 0.2 (see also Eq. (20)). Applying this prerequisite filters out data points for which the $-5/3$ power law generally fails (Grachev *et al.*, 2013, figures 7 and 8).

Note that the 4/3 ratio between $S_v(f)$ and $S_u(f)$ and between $S_w(f)$and $S_u(f)$ within inertial subrange frequencies, Eq. (3), is a stronger indicator of isotropy than the $-5/3$ Kolmogorov power law (Eq. (2)). A $-5/3$ slope in a velocity spectrum can occur even without the local isotropy which it yields Eq. (3) (e.g. see discussion in Biltoft (2001) and Piper and Lundquist (2004) and references therein). According to our data, plots of S_v/S_u and S_w/S_u versus *Ri* and $\zeta = z/L$ show that Eq. (3) is better obeyed for S_v/S_u than for S_w/S_u, and it works better for the upper levels 3–5 than for the lower levels 1–2 (not shown). These results are consistent with the findings by Piper and Lundquist (2004, their fig. 1). Moreover, as *Ri* approaches its canonical 'critical value' of 0.20–0.25 (which corresponds to $\zeta \sim 1$), the predicted relationships for spectral densities (Eq. (3)) tend to level off (especially for S_w/S_u because negative buoyancy inhibits vertical transfer). However, we found that the results obtained are not very sensitive to how the dissipation rate of turbulent kinetic energy ε is evaluated (based solely on the u component or based on the all three wind-speed components).

We also tested an alternative method to filter cases when the $-5/3$ Kolmogorov power law fails. Instead of the restrictions on the gradient and flux Richardson numbers, we imposed the following two prerequisites on the data. First, the data points where the spectral slope in the inertial subrange deviated more than 10% of the theoretical $-5/3$ slope were excluded from the analysis (cf. Hartogensis and De Bruin, 2005, where $\pm 20\%$ was used). Second, to restrict the influence of outliers on the bin-averaging, we imposed a prerequisite proposed and discussed by Grachev *et al.* (2008, 2012). Although these prerequisites differ from the restrictions imposed on the gradient and flux Richardson numbers by Grachev *et al.* (2013) and in the current study, these two approaches are generally equivalent (see Grachev *et al.*, 2013, figures 7 and 8).

3. The MOST formalism

The MOST assumes that the kinematic turbulent momentum flux (or magnitude of the wind stress), $-<u'w'> = \tau$, and turbulent temperature flux, $<w'\theta'> = -H$, along with the buoyancy parameter, $\beta = g/\theta$, are the primary influential variables (also known as governing, scaling, repeating variables or parameters) that 'control' the vertical variation of mean flow and turbulence characteristics in the atmospheric surface layer with height z. Thus, the MOST can be considered as flux-based scaling (e.g. Sorbjan, 2010) where the scaling parameters are

$$\tau, H, \beta. \tag{4}$$

This is the prime similarity hypothesis of Monin and Obukhov (1954).

The flux-based scaling parameters (Eq. (4)) uniquely define a system of three scales that represent length, velocity and temperature:

$$L = \frac{\tau^{3/2}}{\kappa\beta H}, u_* = \sqrt{\tau}, \theta_* = \frac{H}{\sqrt{\tau}}. \tag{5}$$

The length scale L in Eq. (5) is known as the Obukhov length scale (Obukhov, 1946), where, historically, the von Kármán constant $\kappa \approx 0.4$ is included in the definition of L simply by convention. Here and above u_* is the friction velocity, θ is mean potential temperature, g is the acceleration due to gravity, u and w are the longitudinal and vertical velocity components, respectively, prime denotes fluctuations about the mean value and $<>$ is a time or space averaging operator. The sign convention for the temperature flux is $H > 0$ in the SBL.

For simplicity, we consider the case of dry air, otherwise, in the buoyancy term, $\beta<w'\theta'>, \theta$ should be replaced by the virtual potential temperature θ_v. Note, that all variables in this article are expressed in a streamline coordinate system: therefore, $\tau = \tau_x = -<u'w'>$ represents the longitudinal (or downstream) component of the wind stress, whereas, the lateral (or crosswind) stress component $\tau_y = -<v'w'> = 0$ (v' is the lateral velocity components).

Variables that are not listed in Eq. (4) among the scaling parameters are considered as dependent variables. Consider the wind shear $\partial U/\partial z$. According to the MOST, the relevant physical variables for $\partial U/\partial z$ in the stationary, homogeneous atmospheric boundary layer adjacent to a horizontal plane are

$$\partial U/\partial z, \tau, H, \beta, z. \tag{6}$$

These five variables ($n = 5$) involve three fundamental dimensions: length, time, and temperature ($k = 3$). According to Buckingham's Pi theorem (e.g. Monin and Yaglom, 1971; Stull, 1988; Sorbjan, 1989; Barenblatt, 1996; Foken, 2006; Kramm and Herbert, 2009), there are $n - k = 2$ independent dimensionless π groups representing the problem in the general form

$$\pi = f(\pi_1). \tag{7}$$

This statement is also known as the first Pi theorem. The second Pi theorem states that each π group in Eq. (7) is a function of $k = 3$ governing or repeating variables plus one of the remaining variables (the number of repeating variables is equal to the number of fundamental dimensions). In our case, the repeating variables are defined by Eq. (4). Note that the Pi theorem provides only a general approach, and the choice of dimensionless π groups is not unique.

Using the flux-based governing parameters (Eq. (4)), we can now specify the π groups in Eq. (7). The first π group is based on the governing parameters (Eq. (4)) and z that lead to the Monin–Obukhov stability parameter (Monin and Obukhov, 1954); that is, $\pi_1 = \zeta$, where

$$\zeta \equiv \frac{z}{L} = -\frac{z\kappa g<w'\theta'>}{u_*^3\theta}, \tag{8}$$

defined as the ratio of z and the Obukhov length scale, see Eq. (5). The next dimensionless group involves the governing parameters (Eq. (4)) and the vertical gradient of mean wind speed that produces $\pi = \frac{L}{u_*}\frac{\partial U}{\partial z}$.

Now the functional relationship (Eq. (7)) for the non-dimensional vertical gradient of mean wind speed may be expressed as

$$\frac{L}{u_*}\frac{\partial U}{\partial z} = \varphi'_m(\zeta). \tag{9}$$

It is convenient to replace Eq. (9) by the alternative form (Sorbjan, 1989)

$$\frac{\kappa z}{u_*}\frac{\partial U}{\partial z} = \varphi_m(\zeta), \tag{10}$$

where $\varphi_m = \kappa\zeta\varphi'_m$. The von Kármán constant κ on the left-hand side of Eq. (10) is conventionally introduced solely as a matter of convenience such that $\varphi_m(0) = 1$ for neutral conditions ($\zeta \equiv 0$).

Similar to Eq. (6), the relevant physical variables for potential temperature lapse rate, $\partial\theta/\partial z$, on the height z are assumed to be

$$\partial\theta/\partial z, \tau, H, \beta, z. \tag{11}$$

Just as in the previous case, the five independent variables (Eq. (11)) have three fundamental dimensions (i.e. $n = 5$ and $k = 3$) that lead to Eq. (7), where $\pi_1 = \zeta$ and $\pi = \frac{L}{\theta_*}\frac{\partial\theta}{\partial z}$. Similar to Eq. (9), the non-dimensional vertical gradient of the mean potential temperature can be expressed as $\frac{L}{\theta_*}\frac{\partial\theta}{\partial z} = \varphi'_h(\zeta)$, which eventually is equivalent to

$$\frac{\kappa z}{\theta_*}\frac{\partial\theta}{\partial z} = \varphi_h(\zeta), \tag{12}$$

where $\varphi_h = \kappa\zeta\varphi'_h$. For neutral conditions, $\varphi_h(0) = Pr_{t0}$, where $Pr_{t0} \approx 1$ is a constant referred to as the neutral value of the turbulent Prandtl number, defined shortly.

Generally, the MOST predicts that any properly scaled statistics of the turbulence at reference height z are universal functions of the stability parameter (Eq. (8)), $\zeta = z/L$. Specifically, the standard deviation of wind-speed components σ_α and air temperature σ_t are scaled as

$$\frac{\sigma_\alpha}{u_*} = \varphi_\alpha(\zeta), \frac{\sigma_t}{|\theta_*|} = \varphi_t(\zeta), \tag{13}$$

where α (= u, v and w) denotes the longitudinal, lateral or vertical velocity component. In addition, the dissipation rate of turbulent kinetic energy ε in the frameworks of the MOST can be expressed as

$$\frac{\kappa z\varepsilon}{u_*^3} = \varphi_\varepsilon(\zeta). \tag{14}$$

Other widely used stability parameters, along with Eq. (8), are the gradient Richardson number, Ri, defined by

$$Ri = \left(\frac{g}{\theta}\right)\frac{\partial\theta/\partial z}{(\partial U/\partial z)^2} = \frac{\zeta\varphi_h}{\varphi_m^2} \tag{15}$$

and the flux Richardson number, Rf (also known as the mixing efficiency) defined by

$$Rf = -\left(\frac{g}{\theta}\right)\frac{<w'\theta'>}{u_*^2(\partial U/\partial z)} = \frac{\zeta}{\varphi_m}, \tag{16}$$

where both Ri and Rf are expressed in a streamline coordinate system. The ratio of Ri to Rf is the turbulent Prandtl number:

$$Pr_t = \frac{K_m}{K_h} = \frac{<u'w'>(\partial\theta/\partial z)}{<w'\theta'>(\partial U/\partial z)} = \frac{Ri}{Rf} = \frac{\varphi_h}{\varphi_m}, \tag{17}$$

where $K_m = -\frac{<u'w'>}{\partial U/\partial z}$ and $K_h = -\frac{<w'\theta'>}{\partial\theta/\partial z}$ are the turbulent viscosity and the turbulent thermal diffusivity, respectively.

The exact forms of the universal functions (Eqs (10) and (12)–(14)) are not predicted by the MOST and must be determined from measurements. However, the MOST predicts the asymptotic behaviour of these functions under very stable ($\zeta \gg 1$) and extremely unstable stratification (free convection, $\zeta \ll -1$). In the very stable regime, stratification inhibits vertical motions, and the turbulence no longer communicates significantly with the surface (e.g. Monin and Yaglom, 1971), thus z ceases to be a scaling parameter, and this is z-less scaling. In this case, the MOST predicts that various dimensional quantities become independent of z (Obukhov, 1946; Monin and Obukhov, 1954). Specifically, the non-dimensional functions φ'_m, φ'_h, φ_α and φ_t (see Eqs (9) and (13)) cannot contain z in the definition and, therefore, asymptotically approach constant values when $\zeta \gg 1$ (cf. Nieuwstadt, 1984). For the non-dimensional functions φ_m, φ_h and φ_ε, the z-less concept requires that z cancels in Eqs (10), (12) and (14), and linear relationships result. Thus, in the z-less limit,

$$\varphi_x(\zeta) = \beta_x\zeta, \varphi_\alpha(\zeta) = \beta_\alpha, \varphi_t(\zeta) = \beta_t, \tag{18}$$

where β_x ($x = m, h$, and ε), β_α and β_t are numerical coefficients (not to be confused with the buoyancy parameter).

A simple linear interpolation provides blending between neutral and the z-less limits (Eq. (18)) for the $\varphi_x(\zeta)$:

$$\varphi_x(\zeta) = \alpha_x + \beta_x\zeta, \tag{19}$$

where generally $\alpha_m = \alpha_\varepsilon = 1$ and $\alpha_h = Pr_{t0}$. The universal functions $\varphi_\alpha(\zeta)$ and $\varphi_t(\zeta)$, Eq. (13), in the MOST framework are considered to be constant for all $\zeta > 0$.

Although, since the landmark 1968 Kansas field experiment (Businger *et al.*, 1971), Eq. (19) has fit the available experimental data well for $\zeta < 1$ and measurements suggest $\beta_m \approx \beta_h \approx 5$ (Högström, 1988; Sorbjan, 1989; Garratt, 1992; Handorf *et al.*, 1999; Foken, 2008; Wyngaard, 2010), z-less scaling (Eq. (18)) has been questioned for stronger stability, including the limit of very stable stratification. Several studies reported that the stability functions φ_m and φ_h increase more slowly with increasing stability than predicted by the linear Eq. (19). A detailed review of the different nonlinear similarity functions φ_m and φ_h based on data collected in a variety of conditions can be found in Sharan and Kumar (2011).

Several studies attempted to remove the ambiguity between predicted (z-less) and observed behaviour of the universal functions. Grachev *et al.* (2013) argued that the applicability of the MOST (in the local scaling formulation) in stable conditions is limited by the inequalities

$$Ri < Ri_{cr} \text{ and } Rf < Rf_{cr}, \tag{20}$$

where both critical values Ri_{cr} and Rf_{cr} are about 0.20–0.25. Various plots of the universal functions in the literature often contain data points that do not satisfy the condition (20), that is, they do not belong to the MOST.

To evaluate different MOST functions, Grachev *et al.* (2013) suggested separating data points into subcritical and supercritical cases, that is, 'separating the apples from the oranges' based on the prerequisite (Eq. (20)). According to Grachev *et al.* (2013, figures 7 and 8), the upper limit of the MOST in the SBL (Eq. (2)) coincides with the region for which the −5/3 Kolmogorov power law is applicable. In other words, the condition (20) also separates Kolmogorov and non-Kolmogorov turbulence in stratified turbulent shear flows. As mentioned in section 2, in this study, both inequalities (Eq. (20)) with $Ri_{cr} = Rf_{cr} = 0.2$ have been imposed on the data to filter out cases when the Richardson–Kolmogorov cascade is not observed. This practice of separating the data into subcritical and supercritical regimes is consistent with laboratory experiments

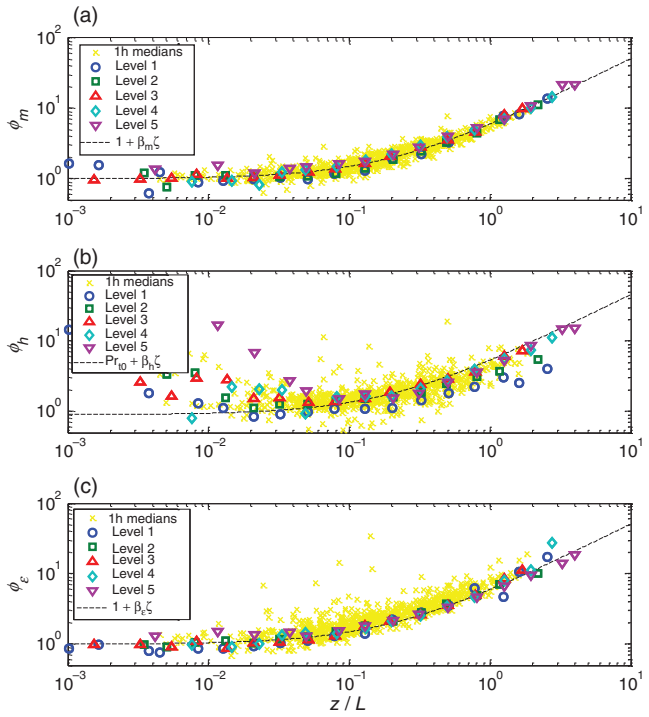

Figure 1. The bin-averaged non-dimensional universal functions (a) φ_m, (b) φ_h and (c) φ_ε for five levels of the main SHEBA tower during the 11 months of measurements plotted versus the Monin–Obukhov stability parameter for local scaling $\zeta = z/L$. Both prerequisites (Eq. (20)) with $Ri_{cr} = Rf_{cr} = 0.2$ have been imposed on the data. The dashed lines are based on $\beta_m = \beta_\varepsilon = 5.0$, $\beta_h = 4.5$ and $Pr_{t0} = \beta_h/\beta_m = 0.9$. Individual 1-h-averaged SHEBA data based on the median fluxes for the five levels are shown as the background × symbols. The SHEBA data with a temperature difference between the air (at median level) and the snow surface less than 0.5 °C have been omitted to avoid the large uncertainty in determining the sensible heat flux. To avoid a possible flux loss caused by inadequate frequency response and sensor separations, a prerequisite that $U > 1$ m s^{-1} has also been imposed.

(e.g. Rohr *et al.*, 1988), theoretical results (Baumert and Peters, 2004; Katul *et al.*, 2014) and field measurements (e.g. Tjernström, 1993).

Figure 1 shows plots of the non-dimensional universal functions φ_m, Eq. (10), φ_h, Eq. (12), and φ_ε, Eq. (14), versus the Monin–Obukhov stability parameter for local scaling $\zeta = z/L$, Eq. (8), when both prerequisites (Eq. (20)) with $Ri_{cr} = Rf_{cr} = 0.2$ have been imposed on the data. The individual 1-h-averaged data, shown in Figure 1 as the background × symbols, are a sample of the available data at one level and show the typical scatter of the data. Implementing the prerequisite (Eq. (20)) reduces the data retained for the analysis from 23% of the original dataset (see section 2) to 17%. According to the SHEBA data, numerical coefficients in Eq. (19) are $\beta_m = 5.0$ (Figure 1(a)), $\beta_h = 4.5$ (Figure 1(b)) and $\beta_\varepsilon = 5.0$ (Figure 1(c)). The numerical coefficients β_m, β_h and β_ε reported here are in close agreement with previously published results (see reviews by Yaglom, 1977; Högström, 1988; Sorbjan, 1989; Garratt, 1992; Hartogensis and De Bruin, 2005; Foken, 2008). For example, Kaimal and Finnigan (1994) recommend $\varphi_m = \varphi_h = \varphi_\varepsilon = 1 + 5\zeta$ for $0 < \zeta < 1$.

Grachev *et al.* (2013, their figure 14) found a numerical coefficient of $\beta_w = 1.3$ in Eq. (13) for the SHEBA. The neutral value of the turbulent Prandtl number in Eq. (19) for $x = h$ has not been specifically determined; instead, we accepted $Pr_{t0} = Pr_t = \beta_h/\beta_m = 0.9$, which coincides with our previous estimate $Pr_t = 0.9$ derived from a plot of Pr_t versus Ri in Sorbjan and Grachev (2010, their figure 2). Further discussion on the turbulent Prandtl number in the SBL can be found in Grachev *et al.* (2007b), Anderson (2009), and references therein.

The universal functions φ_m and φ_ε discussed here are directly associated with the turbulent kinetic energy (TKE) equation (e.g. Garratt, 1992; Kaimal and Finnigan, 1994):

$$\partial <e>/\partial t = -<u'w'>(\partial U/\partial z) + \beta <w'\theta'> - \partial(<w'e> + <w'p'>/\rho)/\partial z - \varepsilon, \qquad (21)$$

where $e = (u'^2 + v'^2 + w'^2)/2$ is TKE and p' is the fluctuation in atmospheric pressure. Assuming steady state ($\partial <e>/\partial t = 0$), Eq. (21) reduces to

$$\varphi_m - \zeta - \varphi_T - \varphi_\varepsilon = 0, \qquad (22)$$

where $\varphi_T = (\kappa z/u_*^3)\partial(<w'e> + <w'p'>/\rho)/\partial z$ is the normalized vertical transport term, and other terms in Eq. (22) are defined by Eqs (10), (8) and (14). The transport term φ_T may be generally neglected (e.g. Monin and Yaglom, 1971) and Eq. (22) can be written as

$$\varphi_m(1 - Rf) - \varphi_\varepsilon = 0, \qquad (23)$$

where Rf is defined by Eq. (16). Note that subsequently specifying φ_ε in Eq. (23), or in its modifications, leads to the, so-called, KEYPS or the O'KEYPS (Businger and Yaglom, 1971) equation for φ_m (named after Obukhov, Kazansky, Ellison, Yamamoto, Panofsky and Sellers) (Monin and Yaglom, 1971; Kramm *et al.*, 1996; Katul *et al.*, 2011).

In the 1968 Kansas data, Wyngaard and Coté (1971) found that, under stable conditions, shear production and viscous dissipation are the dominant terms and they are essentially in balance, that is, $-<u'w'>(\partial U/\partial z) = \varepsilon$ or

$$\varphi_m = \varphi_\varepsilon. \qquad (24)$$

Equation (24) also means that the turbulent transport and the buoyancy production terms are either small or are generally in balance, $\varphi_T = \zeta$ (cf. Eq. (22)). Note that the result $\varphi_\varepsilon \cong \varphi_m$ (or $\beta_\varepsilon \cong \beta_m$) has been known for a long time (at least since the landmark 1968 Kansas field experiment), and our data presented in Figure 1 agree with Eq. (24). In particular, Tjernström (1993, Figure 2) found that the balance $-<u'w'>(\partial U/\partial z) \approx \varepsilon$ is maintained up to $Ri < Ri_{cr} = 0.25$; however, the balance, Eq. (24), abruptly fails when Ri exceeds 0.25. In fact, according to our measurements, an actual difference between β_m and β_ε is within the accuracy of the experimental data. The result (Eq. (24)) will be used in section 4.2.

Concluding this section, we note also that a more general formulation of similarity theory may include additional possible influences on the flux–gradient (or flux–variance, etc.) relationships than the parameters listed in Eq. (4): for example, the Coriolis parameter, boundary layer depth, aerodynamic and scalar roughness lengths, molecular viscosity and thermal conductivity. Such extra parameters would eventually lead to more π groups in Eq. (7) (e.g. Barenblatt, 1996; Mahrt *et al.*, 2003). Furthermore, Klipp and Mahrt (2004, section 8*a*) formulated a generalized *z*-less similarity theory that contains the classical Monin–Obukhov *z*-less asymptote (Eq. (18)) as a special case. According to Klipp and Mahrt (2004), an additional variable $\mathrm{d}\theta/\mathrm{d}z$ should be added to the list (Eq. (6)) (or, equivalently, $\partial U/\partial z$ to the list (Eq. (11))) but z should be dropped to describe flux–profile relationships when $\zeta \gg 1$. Evidently, in the frameworks of the Klipp–Mahrt approach, one may suggest that the variables (Eq. (6)) with an additional parameter $\partial\theta/\partial z$ will lead to Eq. (7), with an additional π group on the right-hand side of the equation, $\pi_2 = \varphi_h'$ ($n = 6$ and $k = 3$). None of these cases are considered here.

4. The N–ε scaling

The flux-based scaling system (Eq. (4)) is not a unique combination of the governing parameters for describing stratified turbulent shear flows (Sorbjan, 2006, 2008, 2010). Here we derive universal functions based on a scaling system that includes the buoyancy frequency N (defined shortly) and the dissipation rate of turbulent kinetic energy ε ('N–ε scaling').

4.1. Dimensional analysis

In oceanography, variables $\partial\theta/\partial z, \varepsilon$ and β or, equivalently,

$$N, \varepsilon, \beta \tag{25}$$

are traditionally used as the governing parameters to describe small-scale turbulence. Here $N = \sqrt{\beta(\partial\theta/\partial z)}$ is the Brunt–Väisälä frequency, or buoyancy frequency. Other variables (e.g. $\partial U/\partial z, \tau, H, \sigma_\alpha, \sigma_t$, etc.) are considered as dependent variables in the framework of N–ε scaling. In the case of humid air or salt water, the buoyancy term $g(\partial\theta/\partial z)/\theta$ appearing in N should be replaced by $g(\partial\theta_v/\partial z)/\theta_v$ or $-g(\partial\rho/\partial z)/\rho$, as discussed earlier ($\rho$ is the potential density). The oceanography community's use of the parameters (Eq. (25)) is primarily associated with the fact that they can be routinely measured in the ocean.

Similar to Eqs (4) and (5), the governing parameters (Eq. (25)) uniquely define a system of three fundamental turbulent scales for the length, velocity and temperature in the framework of the Dougherty–Ozmidov approach:

$$L_{N\varepsilon} = \sqrt{\varepsilon/N^3}, U_{N\varepsilon} = \sqrt{\varepsilon/N}, \theta_{N\varepsilon} = \sqrt{\varepsilon N}/\beta. \tag{26}$$

Obviously $U_{N\varepsilon} = L_{N\varepsilon}N$ and $\theta_{N\varepsilon} = L_{N\varepsilon}(\partial\theta/\partial z)$. Note that the fundamental time-scale is the inverse Brunt–Väisälä frequency, N^{-1}. The buoyancy length scale $L_{N\varepsilon}$ in Eq. (26) was originally suggested by Dougherty (1961) and independently by Ozmidov (1965). Ironically, the length scale $L_{N\varepsilon}$ is widely known as the Ozmidov length scale (e.g. Dillon, 1982; Hunt *et al.*, 1985; Rohr *et al.*, 1988; Galperin *et al.*, 1989; Baumert and Peters, 2000, 2004; Smyth and Moum, 2000; Sorbjan and Balsley, 2008; Mater *et al.*, 2013). Historically the term 'Ozmidov length scale' was introduced by Carl H. Gibson in the oceanographic community (R. V. Ozmidov, 1985; personal communication). The buoyancy velocity and temperature (or density) scales (Eq. (26)) in the SBL were discussed by Gargett *et al.* (1984), Lee (1996) and Sorbjan and Balsley (2008).

Dougherty (1961) considered anisotropy of atmospheric turbulence at heights near 90 km and studied the ratio of $L_{N\varepsilon}$ to the Kolmogorov length scale (see also discussion by Lumley, 1964). Ozmidov (1965, his eq. 5) constructed a buoyancy length scale from $\varepsilon, \partial\rho/\partial z, g/\rho$ to estimate vertical diffusivity in the ocean, and his formulation differs from the canonical relationship $L_{N\varepsilon} = \sqrt{\varepsilon/N^3}$ by only a numerical coefficient. The Dougherty–Ozmidov length scale $L_{N\varepsilon}$ is considered to define the size of the largest eddy that is unaffected by buoyancy in stratified turbulence (e.g. Gibson, 1980).

As mentioned above, variables that are not listed in Eq. (25) among the scaling parameters, are considered as dependent variables. Suppose we are interested in $\partial U/\partial z$ at height z, the relevant physical variables in this case are:

$$\partial U/\partial z, N, \varepsilon, \beta, z. \tag{27}$$

The case of the traditional MOST, with $n = 5$ and $k = 3$ (five independent variables (27) involving three fundamental dimensions), leads to Eq. (7), with $\pi_1 = z/L_{N\varepsilon} \equiv \xi$ and $\pi = \frac{L_{N\varepsilon}}{U_{N\varepsilon}}\frac{\partial U}{\partial z} = \frac{1}{N}\frac{\partial U}{\partial z} = Ri^{-1/2}$, where the gradient Richardson number, Ri, is defined by Eq. (15). It is convenient to write a non-dimensional relationship for dU/dz in the form

$$Ri = \psi_R(\xi). \tag{28}$$

Thus the gradient Richardson number (Eq. (15)) is a universal function of a stability parameter $\xi = z/L_{N\varepsilon}$ defined as the ratio of a reference height z and the Dougherty–Ozmidov length scale.

Applying the above formalism to the turbulent fluxes τ and H (i.e. replacing $\partial U/\partial z$ in Eq. (27) successively by τ and H) results in relationships for the non-dimensional momentum flux $\tau/U_{N\varepsilon}^2$,

$$\frac{\tau N}{\varepsilon} = \psi_m(\xi) \tag{29}$$

and for the non-dimensional temperature flux $H/(U_{N\varepsilon}\theta_{N\varepsilon})$,

$$\frac{\beta H}{\varepsilon} = \psi_h(\xi). \tag{30}$$

Dimensional analysis shows that non-dimensional relationships for the standard deviation of wind-speed components $\sigma_\alpha/U_{N\varepsilon}$ and air temperature $\sigma_t/\theta_{N\varepsilon}$ can be written as

$$\frac{\sigma_\alpha}{\sqrt{\varepsilon/N}} = \psi_\alpha(\xi), \frac{\sigma_t\beta}{\sqrt{\varepsilon N}} = \psi_t(\xi), \tag{31}$$

where $\alpha = u, v$ and w. The non-dimensional relationships for the turbulent viscosity and the turbulent thermal diffusivity are:

$$\frac{K_m N^2}{\varepsilon} = \psi_{Km}(\xi), \frac{K_h N^2}{\varepsilon} = \psi_{Kh}(\xi). \tag{32}$$

Based on Eqs (28)–(30) and the definitions of K_m and K_h, one can show that $\psi_{Km} = \psi_m\psi_R^{1/2} \equiv \psi_m Ri^{1/2}$ and $\psi_{Kh} = \psi_h$ in the case of the dry air. In the general case, $\psi_{Kh} = \psi_h\left(1 + \frac{m}{Bo}\right)$, where Bo is the Bowen ratio (the ratio of the turbulent fluxes of sensible and latent heat) and $m = 0.61\, c_p/L_e \approx 0.075$ (c_p is the heat capacity of air at constant pressure, and L_e is the latent heat of evaporation of water).

The asymptotic behaviour of the universal functions (Eqs (28)–(32)) can be predicted for neutral conditions ($\xi \to 0$) and in the very stable case ($\xi \gg 1$). In the neutral case, various quantities become independent of the buoyancy parameter β (recall that β is included in N), that is, β is no longer a primary scaling variable. This requires that β cancels in Eqs (28)–(32) in the limit $\xi \to 0$; therefore,

$$\begin{aligned}&\psi_R = a_R\xi^{4/3}, \psi_m = a_m\xi^{2/3}, \psi_{Km} = a_{Km}\xi^{4/3},\\ &\psi_{Kh} = a_{Kh}\xi^{4/3}, \psi_\alpha = a_\alpha\xi^{1/3}, \psi_t = a_t\xi.\end{aligned} \tag{33}$$

In the very stable case, various dimensional variables become independent of z (z-less stratification) and the universal functions ((28)–(32)) asymptotically approach constant values when $\xi \gg 1$:

$$\begin{aligned}&\psi_R = b_R, \psi_m = b_m, \psi_{Km} = b_{Km}, \psi_{Kh} = b_{Kh},\\ &\psi_\alpha = b_\alpha, \psi_\alpha = b_\alpha, \psi_t = b_t.\end{aligned} \tag{34}$$

The numerical coefficients in Eqs (33) and (34) will be specified in the next section. Similar to Eq. (19), interpolation forms can be proposed to blend between the neutral (Eq. (33)) and the z-less (Eq. (34)) asymptotic limits.

4.2. Relationships between the universal functions for the flux-based (MOST) and N–ε-based scale systems

Although the derivation of the relationships in the section 4.1 is independent and self-consistent, the universal functions ((28)–(32)) for N–ε scaling can be expressed through the traditional MOST functions defined in section 3 and vice versa. First, the Dougherty–Ozmidov length scale $L_{N\varepsilon} = \sqrt{\varepsilon/N^3}$ is a universal function of the Obukhov length scale $L = \tau^{3/2}/(\kappa\beta H)$ (or, equivalently, $\xi = z/L_{N\varepsilon}$ is a universal function of $\zeta = z/L$). Substituting $\partial\theta/\partial z$ from Eq. (12) and ε from Eq. (14) into $\xi = z/L_{N\varepsilon}$ yields

$$\xi = \frac{(\zeta\varphi_h)^{3/4}}{\kappa\varphi_\varepsilon^{1/2}}, \tag{35}$$

where ζ is defined by Eq. (8). In the neutral limit ($\zeta,\xi \to 0$), Eq. (35), where φ_h and φ_ε are specified by Eq. (19), reduces to $\xi = (Pr_{t0}\zeta)^{3/4}/\kappa$ (i.e. β cancels). In the very stable case ($\zeta,\xi \gg 1$), according to Eqs (19) and (35), $\xi = (\zeta\beta_h^{3/4})/(\kappa\beta_\varepsilon^{1/2})$ (i.e. z cancels). Thus in the z-less regime the Dougherty–Ozmidov length scale is linearly proportional to the Obukhov length.

Similar to Eq. (35), substituting different variables from the appropriate MOST functions (section 3) in the relationships (Eqs (28)–(32)) yields

$$\psi_m = \frac{\sqrt{\zeta\varphi_h}}{\varphi_\varepsilon}, \psi_{Km} = \frac{\zeta\varphi_h}{\varphi_m\varphi_\varepsilon}, \psi_{Kh} = \frac{\zeta}{\varphi_\varepsilon},$$
$$\psi_\alpha = \varphi_\alpha\left(\frac{\zeta\varphi_h}{\varphi_\varepsilon^2}\right)^{1/4}, \psi_t = \varphi_t\left(\frac{\zeta^3}{\varphi_h\varphi_\varepsilon^2}\right)^{1/4}. \quad (36)$$

The universal functions $\psi_R \equiv Ri$ (Eq. (28)), which in the MOST terms are $Ri = \zeta\varphi_h/\varphi_m^2$ (see Eq. (15)) and $\psi_h = \psi_{Kh}/(1 + m/Bo)$, were defined earlier and, for this reason, are not listed in Eq. (36). Thus according to Eq. (36), the universal functions (Eqs (28)–(32)) derived from dimensional reasoning also can be deduced from the traditional MOST functions. This allows recovering numerical coefficients in Eqs (33) and (34).

Combining Eqs (28), (35) and (36) in the neutral limit yields

$$a_R = \kappa^{4/3}, a_m = \kappa^{2/3}, a_{Km} = \kappa^{4/3}, a_{Kh} = \frac{\kappa^{4/3}}{Pr_{t0}},$$
$$a_\alpha = \beta_\alpha\kappa^{1/3}, a_t = \frac{\beta_t\kappa}{Pr_{t0}}. \quad (37)$$

In a similar manner, in the very stable case

$$b_R = \frac{\beta_h}{\beta_m^2} = Ri_{cr}, b_m = \frac{\beta_h^{1/2}}{\beta_\varepsilon}, b_{Km} = \frac{\beta_h}{\beta_m\beta_\varepsilon},$$
$$b_{Kh} = \frac{1}{\beta_\varepsilon}, b_\alpha = \beta_\alpha\left(\frac{\beta_h}{\beta_\varepsilon^2}\right)^{1/4}, b_t = \frac{\beta_t}{(\beta_h\beta_\varepsilon^2)^{1/4}}. \quad (38)$$

Note that in the z-less limit, the vertical gradients of mean wind speed and virtual potential temperature are related as $\beta(\partial\theta_v/\partial z) = b_R(\partial U/\partial z)^2$, that is, $Ri = Ri_{cr} = \beta_h/\beta_m^2$.

Although relationships ((36)) derived in the framework of N–ε scaling are combinations of the traditional Monin–Obukhov functions, they lead to a number of important (and elegant) relationships overlooked previously in the MOST. Based on Eqs (14) and (15) and the experimental fact that $\varphi_\varepsilon \cong \varphi_m$ (see Eq. (24) and the discussion in section 3), the relationships (Eq. (36)) can be rewritten as follows. The universal function ψ_m, Eq. (29), is reduced to

$$\tau N/\varepsilon = \sqrt{Ri}. \quad (39)$$

The equivalent form for the non-dimensional turbulent viscosity (Eq. (32)) is $\psi_{Km} = \psi_m Ri^{1/2}$ or

$$K_m N^2/\varepsilon = Ri. \quad (40)$$

The non-dimensional relationships for the turbulent thermal diffusivity in Eq. (32) also can be written in a similar simple form. Substituting ψ_{Kh} from Eq. (36) into the second Eq. (32) and combining with Eqs (16) and (24) yields

$$K_h N^2/\varepsilon = Rf. \quad (41)$$

Obviously, relationships (Eqs (39)–(41)) are a direct consequence of Eq. (24).

The non-dimensional relationships for the temperature flux (Eq. (30)) is $\psi_h = Rf/(1 + m/Bo)$. Similarly, non-dimensional relationships for the standard deviation of wind-speed components ψ_α and the potential temperature ψ_t in Eq. (36) are reduced to

$$\frac{\sigma_\alpha}{\sqrt{\varepsilon/N}} = \beta_\alpha Ri^{1/4}, \frac{\sigma_t\beta}{\sqrt{\varepsilon N}} = \beta_t Rf/Ri^{1/4}, \quad (42)$$

where $\varphi_\alpha = \beta_\alpha$ and $\varphi_t = \beta_t$. The relationship for ψ_t also can be expressed as $\psi_t = \beta_t(Rf^3/Pr_t)^{1/4} = \beta_t Ri^{3/4}/Pr_t$. Note that Eqs (39)–(42), in contrast to Eqs (28)–(32), do not contain z and, thus, also can be used beyond the surface layer.

Equation (35), which relates the Dougherty–Ozmidov and the Obukhov length scales, may also be simplified. Substituting $\varphi_\varepsilon = \varphi_m$ in Eq. (31) and combining with Eqs (15) and (16) yields

$$L/L_{N\varepsilon} \equiv \xi/\zeta = Ri^{3/4}/(\kappa Rf) = Pr_t/(\kappa Ri^{1/4}) = Pr_t^{3/4}/(\kappa Rf^{1/4}). \quad (43)$$

The other two fundamental scales (Eq. (26)) are related to their Monin–Obukhov counterparts through $u_*/U_{N\varepsilon} = \psi_m^{1/2} = Ri^{1/4}$ and $\theta_*/\theta_{N\varepsilon} = Rf/Ri^{1/4}$.

Although most of the relationships (Eqs (39)–(43)) are extremely simple they are valid for the whole range $0 < Ri < Ri_{cr}$ and $0 < Rf < Rf_{cr}$, where both critical values Ri_{cr} and Rf_{cr} are about 0.20–0.25.

4.3. *Analysis of the SHEBA data*

Measurements of atmospheric turbulence made during the SHEBA are used to plot different universal functions derived earlier in the frameworks of 'N–ε scaling'. Recall that the data in all plots were quality controlled as described in section 2, and the restrictions (Eq. (20)) on the gradient and flux Richardson numbers have been imposed to filter out outliers and data points where the Richardson–Kolmogorov cascade is not observed. Theoretical dashed lines in various plots are based on $\varphi_m = \varphi_\varepsilon = 1 + 5\zeta, \varphi_h = 0.9 + 4.5\zeta$ and $\varphi_w = \beta_w = 1.3$.

Figure 2(a) shows typical values of the Dougherty–Ozmidov length scale $L_{N\varepsilon} = \sqrt{\varepsilon/N^3}$ observed in the stable atmospheric boundary layer. The length scale $L_{N\varepsilon}$ decreases with increasing stability from about 100 to 1 m in the Ri range shown in Figure 2(a). These values are in good agreement with previous estimates of $L_{N\varepsilon}$ by Hunt *et al.* (1985, Sec. 5), Stull (1988, Sec. 12.2.3) and Sorbjan and Balsley (2008, figure 6).

The stability parameter $\xi = z/L_{N\varepsilon}$ versus the Monin–Obukhov stability parameter (Eq. (8)), $\zeta = z/L$, is shown in Figure 2(b), where the dashed line is based on Eq. (35). Note that the plot in Figure 2(b) by definition is not affected by self-correlation because ξ shares no variables with ζ except a reference height z. The greater scatter of points in Figure 2(b) and several other plots in near-neutral conditions results from the relatively small sensible heat flux and unreliable temperature gradient measurements in this case. The relatively large scatter of the bin-averaged data for level 1 and partially for level 2 may be because levels 1 and 2 are located too close to the surface (i.e. within roughness or blending sublayers) and are, consequently, more affected by surface heterogeneity.

The universal function (Eq. (28)) $\psi_R = Ri$ versus $\xi = z/L_{N\varepsilon}$ is plotted in Figure 3(a) in a log–log representation. A similar plot of Rf versus ξ is shown in Figure 3(b). Dashed curves in Figure 3 are based on parametric equations (15), (19) and (35) for panel (a) and on (16), (19) and (35) for panel (b), where ζ is a parameter. In the limit $\xi \to 0$, both curves have a 4/3 slope, that is, $Ri, Rf \propto \xi^{4/3}$ (see also Eqs (33) and (35)).

Plots of the non-dimensional momentum flux (Eq. (29)), $\psi_m = \tau N/\varepsilon$, and the non-dimensional turbulent viscosity (Eq. (32)), $\psi_{Km} = K_m N^2/\varepsilon$, are shown in Figures 4 and 5

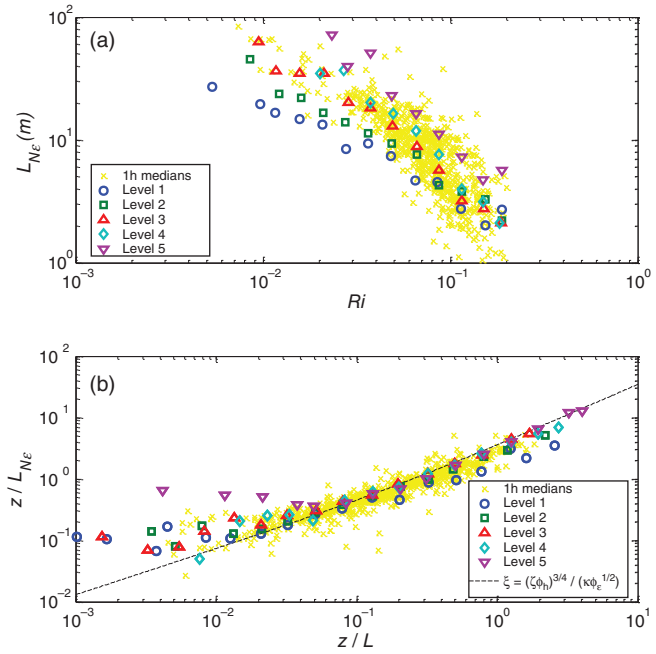

Figure 2. (a) Behaviour of the Dougherty–Ozmidov length scale $L_{N\varepsilon} = \sqrt{\varepsilon/N^3}$ (bin medians) observed in the stable atmospheric boundary layer for SHEBA data plotted against the gradient Richardson number (Eq. (15)). (b) Plot of the bin-averaged stability parameter $\xi = z/L_{N\varepsilon}$ versus the Monin–Obukhov stability parameter (Eq. (8)), $\zeta = z/L$. The dashed line is based on Eqs (35) and (19), where $\beta_m = \beta_\varepsilon = 5.0$, $\beta_h = 4.5$ and $Pr_{t0} = \beta_h/\beta_m = 0.9$. Symbols and notations are the same as in Figure 1.

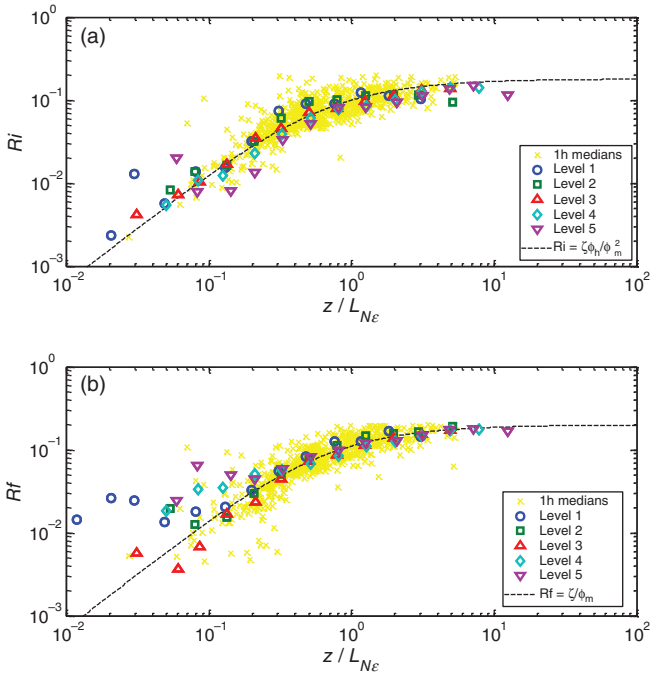

Figure 3. Plots of the bin-averaged (a) gradient Richardson number, Ri, and (b) flux Richardson number, Rf (bin medians), versus the Dougherty–Ozmidov stability parameter $\xi = z/L_{N\varepsilon}$. Dashed curves are based on parametric equations (15), (19) and (35) for (a) and on (16), (19) and (35) for (b), where ζ is a parameter ($\beta_m = \beta_\varepsilon = 5.0$, $\beta_h = 4.5$, and $Pr_{t0} = \beta_h/\beta_m = 0.9$). Symbols and notations are the same as in Figure 1.

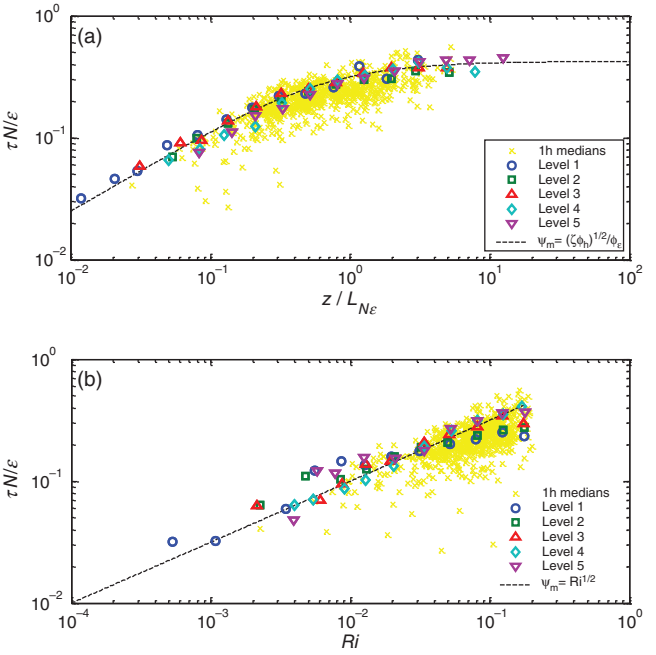

Figure 4. Plots of the bin-averaged non-dimensional momentum flux (Eq. (29)), $\psi_m = \tau N/\varepsilon$, versus (a) the Dougherty–Ozmidov stability parameter, $\xi = z/L_{N\varepsilon}$, and (b) the gradient Richardson number, Ri, see Eq. (39). Symbols and notations are the same as in Figure 1.

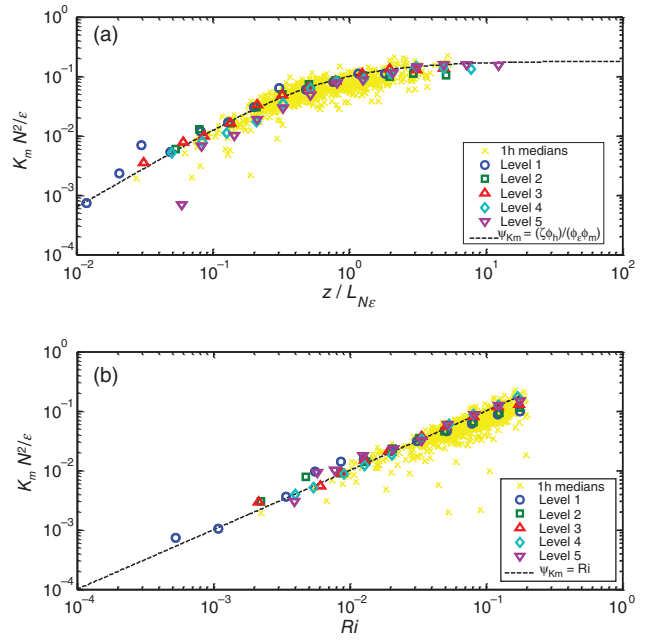

Figure 5. Same as Figure 4 but for the non-dimensional turbulent viscosity (Eq. (32)), $\psi_{Km} = K_m N^2/\varepsilon$.

respectively. Panel (a) in Figures 4 and 5 shows plots of the non-dimensional functions versus ξ, where asymptotic behaviour is described by Eqs (33) and (37) in the limit $\xi \to 0$ and by Eqs (34) and (38) in the very stable case. Panel (b) in Figures 4 and 5 shows plots of ψ_m and ψ_{Km} versus Ri, where the theoretical predictions are described by the simple equations (39) and (40), respectively.

Figure 6(a) shows the non-dimensional turbulent thermal diffusivity (Eq. (32)), $\psi_{Kh} = K_h N^2/\varepsilon$, versus ξ. Asymptotes of $\psi_{Kh}(\xi)$ are described by Eqs (33) and (37) and (34) and (38), and the dashed line is an interpolation curve. In contrast to the non-dimensional turbulent viscosity, which is equal to the gradient Richardson number, $\psi_{Km} = Ri$, Eq. (40), theory predicts that the non-dimensional turbulent thermal diffusivity is equal to the flux Richardson number, $\psi_{Kh} = Rf$, Eq. (41). This dependence is shown in Figure 6(b).

Figures 4(b), 5(b) and 6(b) show good agreement between experimental data and theoretical predictions (Eqs (39)–(41)), which are extremely simple and contain no additional calibration constants. As discussed earlier, these results are a consequence of the approximate local balance between viscous dissipation and production of turbulence kinetic energy by the mean flow: $-\langle u'w'\rangle(\partial U/\partial z) \approx \varepsilon$.

Note that, for practical applications, it is important to know how ψ_{Kh} depends on Ri rather than on Rf. Figure 7(a) plots

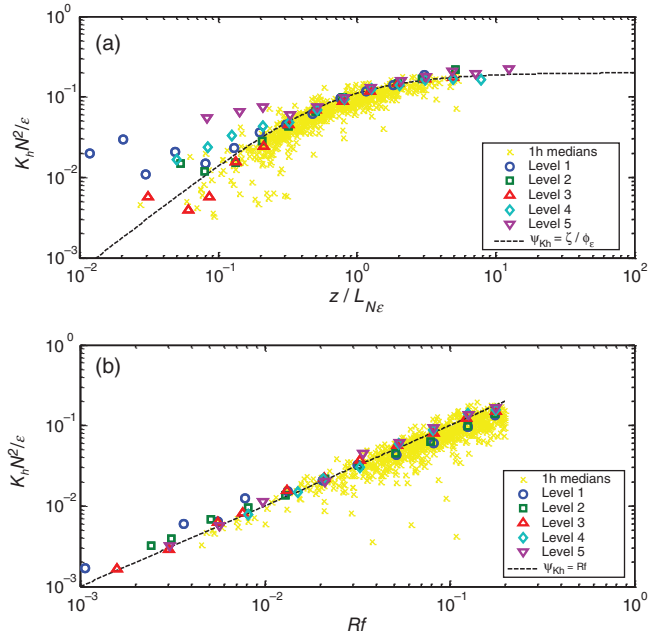

Figure 6. Plots of the bin-averaged non-dimensional turbulent thermal diffusivity (Eq. (32)), $\psi_{Kh} = K_h N^2/\varepsilon$, versus (a) the Dougherty–Ozmidov stability parameter, $\xi = z/L_{N\varepsilon}$, and (b) the flux Richardson number, Rf, see Eq. (40). Symbols and notations are the same as in Figure 1.

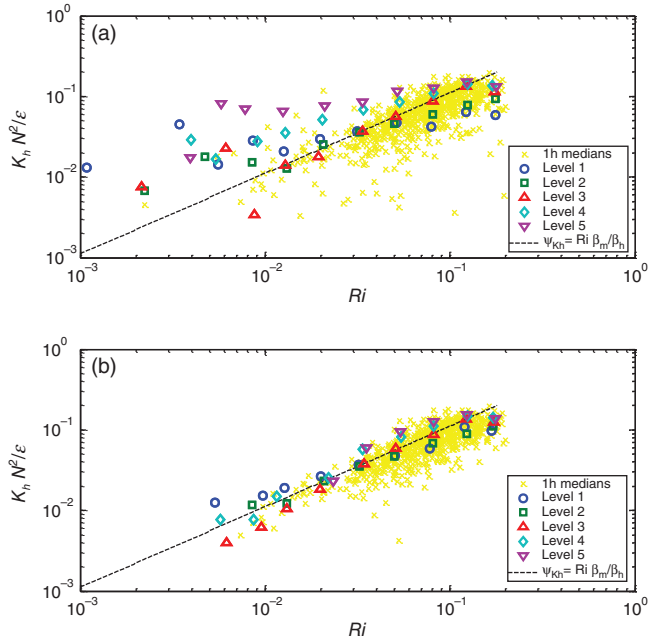

Figure 7. Plots of the bin-averaged non-dimensional turbulent thermal diffusivity (Eq. (32)), $\psi_{Kh} = K_h N^2/\varepsilon$, versus the gradient Richardson number, Ri. (a) No restriction on Ri outliers are applied; (b) the prerequisite (Eq. (44)) has been imposed on the individual data for all five levels and medians ($\times$ symbols) to restrict the influence of the outliers.

the non-dimensional turbulent thermal diffusivity against Ri. According to Figure 7(a), the scatter among different observation levels for ψ_{Kh} is very high, thus, ψ_{Kh} has no universal behaviour if it is plotted versus Ri. This result is somewhat unexpected because a plot of ψ_{Kh} versus Rf (Figure 6(b)) looks 'fine', and Rf is highly correlated with Ri: $Pr_t = Ri/Rf \approx 0.9$ for Ri and $Rf < 0.2$. One may suggest that this behaviour is associated with the influence of outliers on the bin-averaging ('spurious bin-averaging'), as briefly described in Grachev *et al.* (2008, pp. 159–160) and discussed in detail by Grachev *et al.* (2012).

To limit the influence of outliers on the bin-averaging, we have imposed a prerequisite on the data in the form

$$0.5 < Ri/Ri_{\mathrm{SHEBA}} < 2\,, \qquad (44)$$

where $Ri_{\mathrm{SHEBA}} = \zeta \varphi_{h\mathrm{SHEBA}}/\varphi^2_{m\mathrm{SHEBA}}$ is based on the SHEBA profile functions, Eqs (10) and (12), computed for each level separately. Sorbjan (2010) and Sorbjan and Grachev (2010) have also used the prerequisite (Eq. (44)), particularly for their analysis of the flux–profile relationships. Note that implementing the prerequisite (Eq. (44)) in addition to the condition (20) will further reduce the data retained for the analysis from 23% of the original SHEBA dataset (see section 2) to about 11%.

Figure 7(b) shows the same plots as in Figure 7(a) but the prerequisite (Eq. (44)) has been imposed on the individual data for all five levels and medians ($\times$ symbols) to restrict the influence of the outliers. According to Figure 7(b), applying the condition (44) to the data dramatically improved the situation, that is, the plot of ψ_{Kh} versus Ri is now much more consistent with the theoretical predictions (dashed line) as compared with Figure 7(a). Sorbjan (2012) recently also discussed scatter among different observation levels in plots in which Ri is the independent variable. However, the scatter in Figure 7(a) cannot be reduced by using Blackadar's expression for the mixing length instead of κz, as proposed by Sorbjan (2012), simply because Figure 7 contains no z.

A relationship similar to Eq. (41) is widely used in oceanography to calculate the turbulent diffusivity for density K_ρ. The most common method of estimating K_ρ was originally proposed by Osborn (1980) and is based on the stationary TKE equation, assuming a balance between the production of TKE, the buoyancy flux and the dissipation of TKE, Eq. (23). According to Osborn (1980) $K_\rho N^2/\varepsilon = \gamma$, where $\gamma = Rf/(1 - Rf)$ is the mixing efficiency. An upper bound on the mixing efficiency γ is traditionally taken as $\gamma \approx 0.2$, which corresponds to $Rf = Rf_{cr} \approx 0.15$ (Osborn, 1980; Oakey, 1982). In reality, γ is likely to vary with stratification. The mixing efficiency γ and the Osborn method, in general, are further discussed by Peters *et al.* (1988), Weinstock (1992), Moum (1996), Smyth *et al.* (2001) and Lozovatsky and Fernando (2002, 2013), among others.

Figure 8 shows plots of the normalized standard deviation of the vertical wind-speed component, $\psi_w = \sigma_w\sqrt{N/\varepsilon}$ versus $\xi = z/L_{N\varepsilon}$ (Figure 8(a)) and versus Ri (Figure 8(b)). Note that a relationship for the non-dimensional standard deviation of wind-speed components in a general form $\sigma_\alpha/(L_{N\varepsilon}N) = \psi_\alpha(Ri)$ for $\alpha = u$ can be found in Ozmidov (1998, Eq. (10)), although without a specification for $\psi_\alpha(Ri)$. According to our study, $\psi_\alpha(Ri) = \beta_\alpha Ri^{1/4}$, Eq. (42), and $\beta_w = 1.3$ for $\alpha = w$. In fact, Eq. (42) for σ_u in implicit form is contained in Lozovatsky and Ozmidov (1979). According to Lozovatsky and Ozmidov, $\sigma_u/(lN) = 0.8Ri^{-1/2}$ and $\varepsilon/(l^2N^3) = 0.6Ri^{-3/2}$, where l is the turbulence length scale that is associated with the wavenumber of the energy-containing eddies (spectral peak) in the spectrum of the longitudinal velocity component and should be determined experimentally. Combining these two equations from Lozovatsky and Ozmidov leads to $\sigma_u\sqrt{N/\varepsilon} = \beta_u Ri^{1/4}$ with a numerical coefficient approximately equal to 1.

Our relationships (Eq. (42)) are also consistent with previous predictions for various parameters versus Ri ($Ri < Ri_{cr}$) derived in a different context through completely different theoretical means by Rohr *et al.* (1988), Luketina and Imberger (1989), Weinstock (1992), Schumann and Gerz (1995) and Baumert and Peters (2000). In particular, Schumann and Gerz (1995, figure 12) predict $eN/\varepsilon \propto Ri^{1/2}$ for $Ri < Ri_{cr}$, where e is TKE. This result can be derived from Eq. (42) for σ_α. The model by Baumert and Peters (2000) predicts the ratio between the Thorpe length scale (or Ellison length scale) and the Dougherty–Ozmidov length scale, $L_T/L_{N\varepsilon} \propto Ri^{3/4}$ (see also Weinstock, 1992), and the ratio of the Thorpe length scale and the buoyancy length scale, $L_T/L_B \propto Ri^{1/2}$, where $L_B = \sqrt{e}/N$ and $Ri < Ri_{cr} = 0.25$. Obviously, $L_B/L_{N\varepsilon} \propto Ri^{1/4}$ is again consistent with Eq. (42) for σ_α.

5. Final remarks and discussion

We developed a local similarity theory for the stably stratified boundary layer that is based on the Brunt–Väisälä frequency

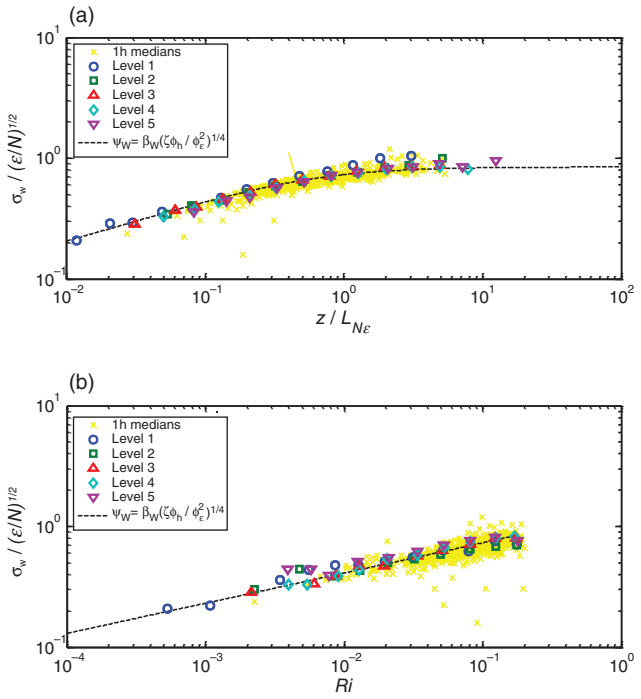

Figure 8. Plots of the bin-averaged non-dimensional standard deviation of the vertical wind-speed component, $\psi_w = \sigma_w\sqrt{N/\varepsilon}$, versus (a) the Dougherty–Ozmidov stability parameter, $\xi = z/L_{N\varepsilon}$, and (b) the gradient Richardson number, Ri. Symbols and notations are the same as in Figure 1.

N, the dissipation rate of TKE ε and the buoyancy parameter β. These three variables are the governing (scaling) parameters, Eq. (25), similar to the turbulent fluxes and β, Eq. (4), used in the traditional MOST. The scaling parameters (Eq. (25)) uniquely define a system of three fundamental scales for the length, velocity and temperature (Eq. (26)). A buoyancy length scale constructed from N and ε,$L_{N\varepsilon} = \sqrt{\varepsilon/N^3}$, was originally suggested by Dougherty (1961) and independently by Ozmidov (1965) and, here, it is referred to as the Dougherty–Ozmidov length scale (in oceanography, it is known as the Ozmidov length scale).

Based on dimensional analysis (Pi theorem) and repeating the Monin–Obukhov formalism described in section 3, but using N and ε instead of the turbulent fluxes, we show that any statistics of the small-scale turbulence properly scaled with Eq. (26) are universal functions of a stability parameter defined as the ratio of height z and the Dougherty–Ozmidov length scale (section 4.1). The Dougherty–Ozmidov length scale $L_{N\varepsilon}$ is uniquely related to the Obukhov length, Eq. (35), and in the limit of z-less stratification, they are linearly proportional to each other. The applicability of the approach as well as the MOST in stable conditions is limited by the inequalities (Eq. (20)), $Ri < Ri_{cr}$ and $Rf < Rf_{cr}$, where both critical values Ri_{cr} and Rf_{cr} are about 0.20–0.25 (cf. Grachev *et al.*, 2013).

Because the scaling system N,ε and β is traditionally used in oceanography, our approach can be considered as a description of the atmospheric turbulence in 'oceanographic language', or as a link between descriptions of atmospheric turbulence and oceanic vertical mixing. Equations (28)–(32), in which $\xi = z/L_{N\varepsilon}$ is the independent variable, can be used to study near-bottom oceanic turbulence (e.g. Peters and Johns, 2006; Lozovatsky *et al.*, 2008, 2010, and references therein) or the oceanic boundary layer under pack ice (McPhee, 2008). It can be assumed that N–ε scaling (section 4) is more suitable for describing the dimensionless oceanic spectra (e.g. Lien and Sanford, 2004; Walter *et al.*, 2011) than the traditional MOST.

Our approach leads to a number of important (and simple) relationships (Eqs (39)–(42)) (in which Ri or Rf are the independent variable) overlooked previously in the MOST and in oceanography (e.g. Eq. (39)). Note that Eqs (39)–(41), in contrast to the traditional MOST relationships, for example, Eqs (10) and (12), have explicit forms and do not contain calibration coefficients. Moreover, Eqs (28)–(32) contain no z and, thus, also can be used far from the surface. This is due to the fact that the relationships (Eqs (39)–(41)) are a consequence of the approximate local balance between production of turbulence by the mean flow and viscous dissipation, Eq. (24).

Although the approach proposed is formally equivalent to the MOST (see section 4.2), it can be used as its replacement in the case when the turbulent fluxes (primary governing variables in the MOST) are not available or cannot be measured directly. Examples of such situations include the previously mentioned small-scale oceanic turbulence or measurements of atmospheric turbulence by a hot-wire anemometer from aircraft, helicopters or balloons (e.g. Muschinski *et al.*, 2001; Sorbjan and Balsley, 2008). Thus the practical importance of the current study is associated with the description of the various small-scale turbulent statistics (including the fluxes) based on measured values of N and ε.

It is apparent that the MOST functions $\varphi_m, \varphi_h, \varphi_\alpha$, etc. are also universal functions of the stability parameter $\xi = z/L_{N\varepsilon}$, and, vice versa, 'new' functions $\psi_m, \psi_h, \psi_\alpha$, etc. are universal functions of the MOST stability parameter (Eq. (8)), $\zeta = z/L$. This is because the Dougherty–Ozmidov length scale $L_{N\varepsilon}$ is uniquely related to the Obukhov length according to Eq. (35). Such a 'hybrid' representation allows plotting functions that by definition are not affected by self-correlation (cf. Grachev *et al.*, 2013, fig. 16). For example, a plot of the MOST non-dimensional vertical gradient of mean wind speed (Eq. (10)), φ_m, versus the Dougherty–Ozmidov stability parameter $\xi = z/L_{N\varepsilon}$ is not affected by self-correlation because φ_m shares no variables with ξ except a reference height z (the plot is not shown here). At the same time, straightforward plots of φ_m versus ζ (Figure 1(a)) and ψ_m versus ξ (Figure 4(a)) are affected by self-correlation.

Local similarity theory based on the scaling system $\{N,\varepsilon,\beta\}$ derived here is not the only option for a reformulation of the MOST. There are many other choices to build up a local similarity theory in the SBL based on different combinations of the scaling parameters. Sorbjan (2006, 2008, 2010) formulated such an approach. The choice of a certain scaling system should be based on the convenience and on the possibility of measuring specific parameters. In addition to the scaling systems by Smeets *et al.* (2000) and Sorbjan (2006, 2008, 2010) mentioned in section 1, the following promising scaling systems are worth mentioning: $\{\sigma_w, \sigma_t, \beta\}$ and $\{\varepsilon, \chi, \beta\}$, where χ is the mean thermal dissipation rate. These scaling systems are associated with the buoyancy length scales $L_{wt} = \sigma_w^2/(\beta\sigma_t)$ and $L_{\varepsilon\chi} = \varepsilon^{5/4}/(\beta^{3/2}\chi^{3/4})$ (Bolgiano–Obukhov length), respectively. Note that the last scaling is equivalent to $\{C_U^2, C_T^2, \beta\}$, where $C_U^2 = 4\alpha\varepsilon^{2/3}$ and $C_T^2 = 4\alpha_T\chi\varepsilon^{-1/3}$ are the structure parameters ($\alpha \approx 0.5$–0.6 is the Kolmogorov constant and $\alpha_T \approx 0.8$) (e.g. Kaimal and Finnigan, 1994).

Acknowledgements

The US National Science Foundation's Office of Polar Programs supported our original SHEBA research. During the current work, NSF also supported AAG and POGP with award ARC 11-07428 and ELA with award ARC 10-19322. AAG also was supported by the US Civilian Research and Development Foundation (CRDF) with award RUG1-2976-ST-10. We thank Evgeni Fedorovich, Iossif Lozovatsky and anonymous reviewers for the helpful comments and suggestions on improving the manuscript. Special thanks go to Boris Galperin for initiating the discussion on the Dougherty–Ozmidov length scale.

References

Albertson JD, Parlange MB, Kiely G, Eichinger WE. 1997. The average dissipation rate of turbulent kinetic energy in the neutral and unstable atmospheric surface layer. *J. Geophys. Res.* **102**: 13423–13432, doi: 10.1029/96JD03346.

Anderson PS. 2009. Measurement of Prandtl number as a function of Richardson number avoiding self-correlation. *Boundary-Layer Meteorol.* **131**: 345–362, doi: 10.1007/s10546-009-9376-4.

Andreas EL, Claffey KJ, Jordan RE, Fairall CW, Guest PS, Persson POG, Grachev AA. 2006. Evaluations of the von Kármán constant in the atmospheric surface layer. *J. Fluid Mech.* **559**: 117–149, doi: 10.1017/S0022112006000164.

Andreas EL, Horst TW, Grachev AA, Persson POG, Fairall CW, Guest PS, Jordan RE. 2010a. Parametrizing turbulent exchange over summer sea ice and the marginal ice zone. *Q. J. R. Meteorol. Soc.* **136**: 927–943, doi: 10.1002/qj.618.

Andreas EL, Persson POG, Jordan RE, Horst TW, Guest PS, Grachev AA, Fairall CW. 2010b. Parameterizing turbulent exchange over sea ice in winter. *J. Hydrometeorol.* **11**: 87–104, doi: 10.1175/2009JHM1102.1.

Andreas EL, Jordan RE, Mahrt L, Vickers D. 2013. Estimating the Bowen ratio over the open and ice-covered ocean. *J. Geophys. Res. Oceans* **118**: 4334–4345, doi: 10.1002/jgrc.20295.

Barenblatt GI. 1996. *Scaling, Self-similarity, and Intermediate Asymptotics.* Cambridge University Press: Cambridge, UK.

Baumert H, Peters H. 2000. Second-moment closures and length scales for weakly stratified turbulent shear flows. *J. Geophys. Res.* **105**: 6453–6468, doi: 10.1029/1999JC900329.

Baumert H, Peters H. 2004. Turbulence closure, steady state, and collapse into waves. *J. Phys. Oceanogr.* **34**: 505–512.

Biltoft CA. 2001. Some thoughts on local isotropy and the 4/3 lateral to longitudinal velocity spectrum ratio. *Boundary-Layer Meteorol.* **100**: 393–404, doi: 10.1023/A:1019289915930.

Businger JA, Yaglom AM. 1971. Introduction to Obukhov's paper on 'Turbulence in an atmosphere with a non-uniform temperature'. *Boundary-Layer Meteorol.* **2**: 3–6.

Businger JA, Wyngaard JC, Izumi Y, Bradley EF. 1971. Flux–profile relationships in the atmospheric surface layer. *J. Atmos. Sci.* **28**: 181–189.

Chamecki M, Dias NL. 2004. The local isotropy hypothesis and the turbulent kinetic energy dissipation rate in the atmospheric surface layer. *Q. J. R. Meteorol. Soc.* **130**: 2733–2752, doi: 10.1256/qj.03.155.

Dillon TM. 1982. Vertical overturns: A comparison of Thorpe and Ozmidov length scales. *J. Geophys. Res.* **87**: 9601–9613, doi: 10.1029/JC087iC12p09601.

Dougherty JP. 1961. The anisotropy of turbulence at the meteor level. *J. Atmos. Terr. Phys.* **21**: 210–213.

Foken T. 2006. 50 years of the Monin–Obukhov similarity theory. *Boundary-Layer Meteorol.* **119**: 431–447, doi: 10.1007/s10546-006-9048-6.

Foken T. 2008. *Micrometeorology*. Springer-Verlag: Berlin and Heidelberg, Germany.

Galperin B, Rosati A, Kantha LH, Mellor GL. 1989. Modeling rotating stratified turbulent flows with application to oceanic mixed layers. *J. Phys. Oceanogr.* **19**: 901–916.

Gargett AE, Osborn TR, Nasmyth PW. 1984. Local isotropy and the decay of turbulence in a stratified fluid. *J. Fluid Mech.* **144**: 231–280, doi: 10.1017/S0022112084001592.

Garratt JR. 1992. *The Atmospheric Boundary Layer*. Cambridge University Press: Cambridge, UK.

Gibson CH. 1980. Fossil turbulence, salinity and vorticity turbulence in the ocean. In *Marine Turbulence*, Nihuol JCJ. (ed.) *Oceanographic Series* **16**: 221–257. Elsevier: Amsterdam.

Grachev AA, Fairall CW, Persson POG, Andreas EL, Guest PS. 2005. Stable boundary-layer scaling regimes: The SHEBA data. *Boundary-Layer Meteorol.* **116**: 201–235, doi: 10.1007/s10546-004-2729-0.

Grachev AA, Andreas EL, Fairall CW, Guest PS, Persson POG. 2007a. SHEBA flux–profile relationships in the stable atmospheric boundary layer. *Boundary-Layer Meteorol* **124**: 315–333, doi: 10.1007/s10546-007-9177-6.

Grachev AA, Andreas EL, Fairall CW, Guest PS, Persson POG. 2007b. On the turbulent Prandtl number in the stable atmospheric boundary layer. *Boundary-Layer Meteorol* **125**: 329–341, doi: 10.1007/s10546-007-9192-7.

Grachev AA, Andreas EL, Fairall CW, Guest PS, Persson POG. 2008. Turbulent measurements in the stable atmospheric boundary layer during SHEBA: Ten years after. *Acta Geophys.* **56**: 142–166, doi: 10.2478/s11600-007-0048-9.

Grachev AA, Andreas EL, Fairall CW, Guest PS, Persson POG. 2012. Outlier problem in evaluating similarity functions in the stable atmospheric boundary layer. *Boundary-Layer Meteorol.* **144**: 137–155, doi: 10.1007/s10546-012-9714-9.

Grachev AA, Andreas EL, Fairall CW, Guest PS, Persson POG. 2013. The critical Richardson number and limits of applicability of local similarity theory in the stable boundary layer. *Boundary-Layer Meteorol.* **147**: 51–82, doi: 10.1007/s10546-012-9771-0.

Handorf D, Foken T, Kottmeier C. 1999. The stable atmospheric boundary layer over an Antarctic ice sheet. *Boundary-Layer Meteorol.* **91**: 165–186, doi: 10.1023/A:1001889423449.

Hartogensis OK, De Bruin HAR. 2005. Monin–Obukhov similarity functions of the structure parameter of temperature and turbulent kinetic energy dissipation rate in the stable boundary layer. *Boundary-Layer Meteorol.* **116**: 253–276, doi: 10.1007/s10546-004-2817-1.

Högström U. 1988. Non-dimensional wind and temperature profiles in the atmospheric surface layer: A re-evaluation. *Boundary-Layer Meteorol.* **42**: 55–78.

Hunt JCR, Kaimal JC, Gaynor JE. 1985. Some observations of turbulence structure in stable layers. *Q. J. R. Meteorol. Soc.* **111**: 793–815, doi: 10.1002/qj.49711146908.

Kaimal JC, Finnigan JJ. 1994. *Atmospheric Boundary Layer Flows: Their Structure and Measurements*. Oxford University Press: New York, NY and Oxford, UK.

Katul GG, Konings AG, Porporato A. 2011. Mean velocity profile in a sheared and thermally stratified atmospheric boundary layer. *Phys. Rev. Lett.* **107**: 268502, doi: 10.1103/PhysRevLett.107.268502.

Katul GG, Porporato A, Shah S, Bou-Zeid E. 2014. Two phenomenological constants explain similarity laws in stably stratified turbulence. *Phys. Rev. E* **89**: 023007, doi: 10.1103/PhysRevE.89.023007.

Klipp CL, Mahrt L. 2004. Flux–gradient relationship, self-correlation and intermittency in the stable boundary layer. *Q. J. R. Meteorol. Soc.* **130**: 2087–2103, doi: 10.1256/qj.03.161.

Kramm G, Herbert F. 2009. Similarity hypotheses for the atmospheric surface layer expressed by non-dimensional characteristic invariants – a review. *Open Atmos. Sci. J.* **3**: 48–79, doi: 10.2174/1874282300903010048.

Kramm G, Herbert F, Bernhardt K, Müller H, Werle P, Foken T, Richter SH. 1996. Stability functions for momentum, heat and water vapour and the vertical transport of TKE and pressure fluctuations estimated from measured vertical profiles of wind speed, temperature and humidity. *Beitr. Phys. Atmos.* **69**: 463–475.

LeeX. 1996. Turbulence spectra and eddy diffusivity over forests. *J. Appl. Meteorol.* **35**: 1307–1318.

Lien R, D'Asaro EA. 2006. Measurement of turbulent kinetic energy dissipation rate with a Lagrangian float. *J. Atmos. Oceanic Technol.* **23**: 964–976, doi: 10.1175/JTECH1890.1.

Lien R, Sanford TB. 2004. Turbulence spectra and local similarity scaling in a strongly stratified oceanic bottom boundary layer. *Cont. Shelf Res.* **24**: 375–392, doi: 10.1016/j.csr.2003.10.007.

Lozovatsky ID, Fernando HJS. 2002. Mixing on a shallow shelf of the Black Sea. *J. Phys. Oceanogr.* **32**: 945–956.

Lozovatsky ID, Fernando HJS. 2013. Mixing efficiency in natural flows. *Phil. Trans. R. Soc. A* **371**: 20120213, doi: 10.1098/rsta.2012.0213.

Lozovatsky ID, Ozmidov RV. 1979. Relationship between characteristics of small-scale turbulence and stratification in the ocean. *Oceanologia* **19**: 649–655 (English Edition).

Lozovatsky ID, Liu Z, Wei H, Fernando HJS. 2008. Tides and mixing in the northwestern East China Sea. Part II: The near-bottom turbulence. *Cont. Shelf Res.* **28**: 338–350, doi: 10.1016/j.csr.2007.08.007.

Lozovatsky I, Roget E, Planella J, Fernando HJS, Liu Z. 2010. Intermittency of near-bottom turbulence in tidal flow on a shallow shelf. *J. Geophys. Res.* **115**: C05006, doi: 10.1029/2009JC005325.

Luketina DA, Imberger J. 1989. Turbulence and entrainment in a buoyant surface plume. *J. Geophys. Res.* **94**: 12619–12636, doi: 10.1029/JC094iC09p12619.

Lumley JL. 1964. The spectrum of nearly inertial turbulence in a stably stratified fluid. *J. Atmos. Sci.* **21**: 99–102.

Mahrt L, Vickers D, Frederickson P, Davidson K, Smedman A-S. 2003. Sea-surface aerodynamic roughness. *J. Geophys. Res.* **108**: 3171, doi:10.1029/2002JC001383.

Mater BD, Schaad SM, Venayagamoorthy SK. 2013. Relevance of the Thorpe length scale in stably stratified turbulence. *Phys. Fluids* **25**: 076604, doi: 10.1063/1.4813809.

McPhee MG. 2008. *Air–Ice–Ocean Interaction: Turbulent Ocean Boundary Layer Exchange Processes.* Springer: New York, NY.

Monin AS, Obukhov AM. 1954. Basic laws of turbulent mixing in the surface layer of the atmosphere. *Trudy Geofiz. Inst. Acad. Nauk SSSR* **24**: 163–187.

Monin AS, Yaglom AM. 1971. *Statistical Fluid Mechanics: Mechanics of Turbulence*, Vol. 1. MIT Press: Cambridge, MA.

Moum JN. 1996. Efficiency of mixing in the main thermocline. *J. Geophys. Res.* **101**: 12057–12069, doi: 10.1029/96JC00508.

Muschinski A, Frehlich R, Jensen M, Hugo R, Hoff A, Eaton F, Balsley B. 2001. Fine-scale measurements of turbulence in the lower troposphere: An intercomparison between a kite- and balloon-borne, and a helicopter-borne measurement system. *Bound.-Layer Meteorol.* **98**: 219–250, doi: 10.1023/A:1026520618624.

Nieuwstadt FTM. 1984. The turbulent structure of the stable, nocturnal boundary layer. *J. Atmos. Sci.* **41**: 2202–2216.

Oakey NS. 1982. Determination of the rate of dissipation of turbulent energy from simultaneous temperature and velocity shear microstructure measurements. *J. Phys. Oceanogr.* **12**: 256–271.

Obukhov AM. 1946. Turbulence in an atmosphere with a non-uniform temperature. *Tr. Inst. Teor. Geophys. Akad. Nauk SSSR* **1**: 95–115 (translation in: *Boundary-Layer Meteorol.,* 1971, **2**: 7–29).

Osborn TR. 1980. Estimates of the local rate of vertical diffusion from dissipation measurements. *J. Phys. Oceanogr.* **10**: 83–89.

Ozmidov RV. 1965. On the turbulent exchange in a stably stratified ocean. *Izv. Atmos. Ocean Phys.* **1**: 493–497 (English Edition).

Ozmidov RV. 1998. Vertical exchange in the ocean. *Phys. Oceanogr.* **9**: 417–425, doi: 10.1007/BF02524658 (English Edition).

Persson POG. 2012. Onset and end of the summer melt season over sea ice: Thermal structure and surface energy perspective from SHEBA. *Clim. Dyn.* **39**: 1349–1371, doi: 10.1007/s00382-011-1196-9.

Persson POG, Fairall CW, Andreas EL, Guest PS, Perovich DK. 2002. Measurements near the Atmospheric Surface Flux Group tower at SHEBA: Near-surface conditions and surface energy budget. *J. Geophys. Res.* **107**: 8045, doi: 10.1029/2000JC000705.

Peters H, Johns WE. 2006. Bottom layer turbulence in the red sea outflow plume. *J. Phys. Oceanogr.* **36**: 1763–1785, doi: 10.1175/JPO2939.1.

Peters H, Gregg MC, Toole JM. 1988. On the parameterization of equatorial turbulence. *J. Geophys. Res.* **93**: 1199–1218, doi: 10.1029/JC093iC02p01199.

Piper M, Lundquist JK. 2004. Surface layer turbulence measurements during a frontal passage. *J. Atmos. Sci.* **61**: 1768–1780.

Rohr JJ, Itsweire EC, Helland KN, Van Atta CW. 1988. Growth and decay of turbulence in a stably stratified shear flow. *J. Fluid Mech.* **195**: 77–111.

Sanz Rodrigo J, Anderson PS. 2013. Investigation of the stable atmospheric boundary layer at Halley Antarctica. *Boundary-Layer Meteorol.* **148**: 517–539, doi: 10.1007/s10546-013-9831-0.

Schumann U, Gerz T. 1995. Turbulent mixing in stably stratified shear flows. *J. Appl. Meteorol.* **34**: 33–48.

Sharan M, Kumar P. 2011. Estimation of upper bounds for the applicability of nonlinear similarity functions for non-dimensional wind and temperature profiles in the surface layer in very stable conditions. *Proc. R. Soc. A* **467**: 473–494, doi: 10.1098/rspa.2010.0220.

Smeets CJPP, Duynkerke PG, Vugts HF. 2000. Turbulence characteristics of the stable boundary layer over a mid-latitude glacier. Part II: Pure katabatic forcing conditions. *Boundary-Layer Meteorol.* **97**: 73–107, doi: 10.1023/A:1002738407295.

Smyth WD, Moum JN. 2000. Length scales of turbulence in stably stratified mixing layers. *Phys. Fluids* **12**: 1327–1342.

Smyth WD, Moum JN, Caldwell DR. 2001. The efficiency of mixing in turbulent patches: Inferences from direct simulations and microstructure observations. *J. Phys. Oceanogr.* **31**: 1969–1992.

Sorbjan Z. 1989. *Structure of the Atmospheric Boundary Layer*. Prentice-Hall: Englewood Cliffs, NJ.

Sorbjan Z. 2006. Local structure of turbulence in stably-stratified boundary layers. *J. Atmos. Sci.* **63**: 1526–1537.

Sorbjan Z. 2008. Gradient-based similarity in the atmospheric boundary layer. *Acta Geophys.* **56**: 220–233, doi: 10.2478/s11600-007-0036-0.

Sorbjan Z. 2010. Gradient-based scales and similarity laws in the stable boundary layer. *Q. J. R. Meteorol. Soc.* **136**: 1243–1254, doi: 10.1002/qj.638.

Sorbjan Z. 2012. The height correction of similarity functions in the stable boundary layer. *Boundary-Layer Meteorol.* **142**: 21–31, doi 10.1007/s10546-011-9653-x.

Sorbjan Z, Balsley BB. 2008. Microstructure of turbulence in the stably stratified boundary layer. *Boundary-Layer Meteorol.* **129**: 191–210, doi: 10.1007/s10546-008-9310-1.

Sorbjan Z, Grachev AA. 2010. An evaluation of the flux–gradient relationship in the stable boundary layer. *Boundary-Layer Meteorol.* **135**: 385–405, doi: 10.1007/s10546-010-9482-3.

Stull RB. 1988. *An Introduction to Boundary-Layer Meteorology*. Kluwer Academic Publishers: Boston, MA.

Tjernström M. 1993. Turbulence length scales in stably stratified free shear flow analyzed from slant aircraft profiles. *J. Appl. Meteorol.* **32**: 948–963.

Vickers D, Mahrt L. 1997. Quality control and flux sampling problems for tower and aircraft data. *J. Atmos. Oceanic Technol.* **14**: 512–526.

Walter RK, Nidzieko NJ, Monismith SG. 2011. Similarity scaling of turbulence spectra and cospectra in a shallow tidal flow. *J. Geophys. Res.* **116**: C10019, doi: 10.1029/2011JC007144.

Weinstock J. 1992. Vertical diffusivity and overturning length in stably stratified turbulence. *J. Geophys. Res.* **97**: 12653–12658, doi: 10.1029/92JC01099.

Wyngaard JC. 2010. *Turbulence in the Atmosphere*. Cambridge University Press: New York, NY.

Wyngaard JC, Coté OR. 1971. The budgets of turbulent kinetic energy and temperature variance in the atmospheric surface layer. *J. Atmos. Sci.* **28**: 190–201.

Yaglom AM. 1977. Comments on wind and temperature flux–profile relationships. *Boundary-Layer Meteorol.* **11**: 89–102.

